Proceedings from the University of Washington
School of Oceanography Senior Thesis, Academic Year 2012-2013

Underway O_2/Ar-estiment net community production across the Kuroshio Extension and impact on winter pCO_2 drawdown

Diane Perry[1]

[1]*University of Washington, School of Oceanography,*
Box 355351, Seattle, Washington 98195
[*]*perryd2@uw.edu*
Received June 2013

NONTECHNICAL SUMMARY

Global warming is a hot topic in global society. Net carbon dioxide (CO_2) flux enters the ocean due to partial pressure deviations. Net community production (NCP) lowers surface ocean pCO_2, but the degree to which remains a fundamental question. Continuous data were collected across the Kuroshio Extension during winter to estimate NCP and its impact on the region's historic pCO_2 drawdown. Large variation in mixed layer (ML) mass balance terms obscured estimation of NCP.

ABSTRACT

The importance of biological versus physical processes influencing oceanic drawdown of *p*CO2 remains unclear. Continuous and discrete O_2 and O_2/Ar measurements were sampled during a late winter transect across the KE (~30ºN 146ºE to 41ºN 150ºE). Average saturation values for O_2 and O_2/Ar were found to be -4.4 ± 1.2% and -4.4 ± 1.4% respectively. Entrainment flux and air-sea gas exchange flux terms were accounted for in a ML mass balance. O_2 and O_2/Ar entrainment fluxes were found to be -93 ± 89 and -76 mmol C m^{-2} d^{-1}. O_2, and O_2/Ar air-water fluxes were both equal to 70 ± 80 mmol C m^{-2} d^{-1}. High variation obscured NCP estimation. Future studies within the KE must take into account entrainment fluxes to better constrain the mixed layer mass balance. Argo floats deployed within the region will provide a five-year dataset crucial to developing these constraints.

Air-sea CO_2 flux is proportional to the air-sea difference in CO_2 (ΔpCO_2); therefore, predicting future climate and ocean chemistry relies on quantitatively understanding processes controlling surface ocean pCO_2.

The North Pacific basin hosts a large net annual seaward pCO_2 flux (Takahashi et al., 2009). Largest flux values (≥ 1.7 mol C m^{-2} yr^{-1}) reside within a subarctic-subtropical transitional zone (~30ºN to 40-45ºN) basin-wide (Figure 1; Ayers and Lozier, 2012). A steep sea surface height gradient across the North Pacific Transition Zone (NPTZ) generates a strong geostrophic eastward current called the Kuroshio Extension (Qiu et al., 2007). A chlorophyll front with enhanced production is associated with the NPTZ (Polovina, 2001; Juranek, 2007; Howard et al., 2010). Takahashi et al. (2009) propose winter cooling and enhanced production along the chlorophyll front drive large CO_2 flux into the NPTZ. Ayers and Lozier (2012) suggest steady geostrophic divergence of dissolved inorganic carbon (DIC) is a greater force in addition to temperature and biological effects. The biological pump photosynthetically fixes CO_2 and exports organic carbon to the deep ocean (Volk and

Hoffert, 1985). One mole of carbon exported equals one mole decrease in surface DIC. Biological pump mediated reduction in surface pCO_2 remains poorly constrained despite its predicted dominance (Emerson et al., 1997; Takahashi et al., 2009; Ayers and Lozier, 2012). Net community production is equal to the biological pump under steady-state conditions. O_2/Ar ratio measurements are routinely used to estimate NCP (Juranek, 2007; Howard et al., 2010).

This thesis analyzes continuous underway surface O_2/Ar measurements determined by equilibrator inlet mass spectrometry (EIMS) across the Kuroshio Extension (KE) in late-winter to attempt to estimate NCP and its contribution to the large regional net drawdown of pCO_2. Limitations of this method in regions with large entrainment fluxes are then discussed.

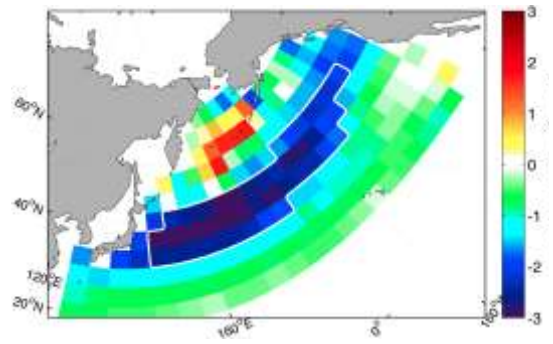

Figure 1. Net annual flux of CO_2 in mol m^{-2} yr^{-1} from Ayers and Lozier (2010). Cooler colors represent larger downward (negative) flux rates. The region associated with the NPTZ with flux rates greater than or equal to -1.7 mol m^{-2} yr^{-1} from Takahashi et al. (2009) data set are traced with a white outline.

METHODS

Field and Laboratory Methods—Samples were collected over 22 days during a northward and southward transect across the KE (Fig. 2). A 24 Niskin bottle conductivity-temperature-depth (CTD) rosette was deployed along with an autonomous Argo float every northward latitude degree (13 stations) and southward calibration of an Argo float (10 stations) for a total of 23 stations. Duplicate O_2/Ar and O_2 discrete samples were collected with at least one sample pair from below the ML and the rest providing good data replication within the ML. Only underway data from the northward leg (~30ºN 146ºE to 41ºN 150ºE) were considered due to erroneous salinity data during southward transit. Underway samples were collected autonomously every 3 minutes (27 Feb. 2013 through 16 Mar. 2013). Sea surface temperature (SST), sea surface salinity (SSS), dissolved O_2, and wind speed were recorded by the *R/V Melville's* underway seawater inlet and metrological systems. O_2/Ar measurements were sampled from the seawater inlet via EIMS following Cassar et al. (2009). Ambient air was pumped every 2.5 h into the mass spectrometer for 30 minutes to correct the O_2/Ar current ratio. All underway data collected during air correction and 6 minutes subsequent were disregarded.

Discrete O_2/Ar samples were taken in duplicate every 6-8 hours following the methods of Emerson et al. (1995). 500 ml volume calibrated glass flasks with 9 mm Louwers O-ring sealing valves were poisoned with $HgCl_2$, evacuated, and the necks filled with CO_2 in the lab prior to shipment to Japan. At sea, ~250 ml of seawater was drawn into an evacuated flask that was then sealed to the second O-ring. Seawater was rinsed from the neck between the two O-rings. The neck was then dried and filled with CO_2 for storage. Back at the University of Washington laboratory, O_2/Ar flasks were weighed and submersed in a water bath at constant temperature overnight to equilibrate gases between the sample headspace and water. Most of the water was pumped from the flasks leaving a few ml to not to pump out the headspace gas. The sample gas was cryogenically pumped through liquid nitrogen to remove CO_2 and water vapor. It was then pumped into a steel 'finger' in liquid helium. It was spiked with ^{36}Ar then removed from the liquid helium and left for 4 h before being analyzed on a Finnigan 253 mass spectrometer by the intrepid lab technician Charles Stump. Discrete O_2 samples were titrated aboard ship by the modified Winkler method (Carpenter 1965).

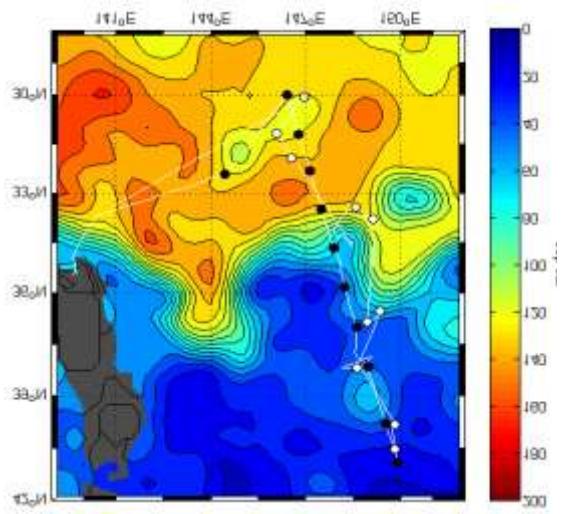

Figure 2. Courtesy of Hilary Palvesky and Byron Kilbourne contour map of SSH. Warmer colors are higher cooler are lower. Black dots are northward CTD stations and white dots are southward CTD stations. Data were collected underway following the white lines.

Terminology—Deviations in air-sea gas equilibrium (ΔC) for O_2 and O_2/Ar were calculated at all underway points as percent saturation (Eq. 1).

$$\Delta C = \frac{C - C_{sat}}{C_{sat}} \times 100\% \quad (1)$$

Negative ΔC indicates undersaturation where C_{sat} equals gas concentration at saturation, and C represents gas concentration measured in-situ. Oxygen saturations were calculated from equation eight in Garcia and Gordon (1992) with Benson and Krause (1984) coefficients. Argon saturation calculations use the laboratory measurements of Hamme and Emerson (2004). The O_2/Ar method assumes oxygen molecular diffusion and solubility coefficients are identical to argon, which is biologically inert. The difference in the degree of saturation between ML oxygen and argon leaves net oxygen produced biologically (NOP). Multiplying NOP by 1.4 stoichiometrically equals NCP. Gas transfer velocities were calculated at all northward underway points for NCP estimation

Calibration—Discrete O_2/Ar samples were returned to University of Washington and analyzed as in Howard et al. (2010). A multiplicative offset of 0.860 ± 0.006 µmol kg^{-1} calibrated laboratory with EIMS determined O_2/Ar ratios (n=7). Discrete and continuous O_2 measurements were calibrated using a linear regression, and agreed within a root mean square of 3.629 µmol kg^{-1} (Fig. 3). Underway and Niskin surface O_2 concentration were matched by timestamp to check for respiration in the underway line (Juranek et al., 2010). Offsets (1.77 ± 1.37 µmol kg^{-1}) were consistent suggesting no underway respiration bias.

RESULTS

Density ranged 25.2 ± 0.1 to 26.5 ± 0.1 (sigma-theta) crossing the subarctic-subtropical boundary (Fig. 4C). Underway Δ(O_2/Ar) and ΔO_2 remained negative across the northward transect averaging -4.43 ± 1.22% and -4.42 ± 1.37% respectively (Fig. 4). Nine oxygen profiles and one O_2/Ar profile were analyzed within the thesis timeframe. ΔO_2 and ΔO_2/Ar percent decreased about 0.05% m^{-1} within the first 125 m of all oxygen profile pycnoclines. ML depth ranged 56.2 to 373 m averaging roughly 193 m (n=8) along the northward track. Dissolved oxygen and argon remained undersaturated in all ML profile and underway data.

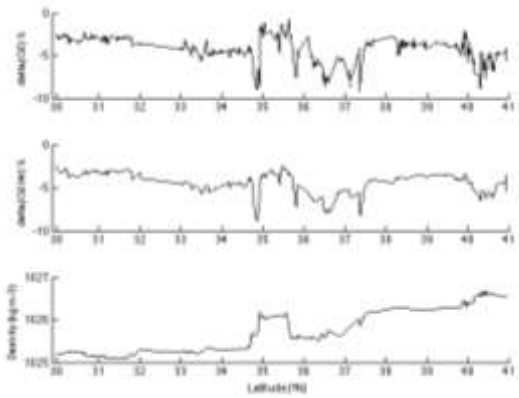

Figure 3. Underway data graphed over latitude of oxygen degree of saturation (top), oxygen/argon degree of saturation (middle), and density (bottom). Values are negative and therefore undersaturated.

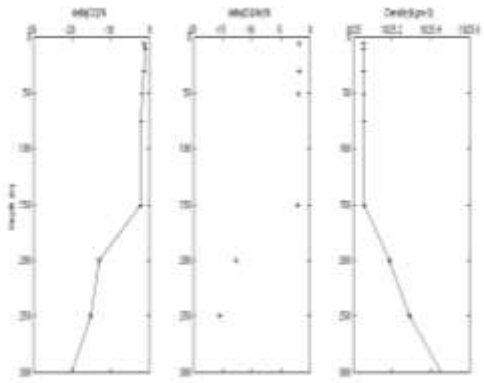

Figure 4 $\Delta O_2/Ar$ profile analyzed at UW (middle), density (right), and degree of oxygen saturation (left). Two $\Delta O_2/Ar$ points are present below the mixed layer.

Adhering to steady-state isolated ML assumptions, undersaturated $\Delta(O_2/Ar)$ must be interpreted as net heterotrophy. However, previous findings of increased production along the NPTZ render a net heterotrophy conclusion suspect (Polovina, 2001; Juranek, 2007; Howard et al., 2010). Winter ML deepening causes entrainment in which low ΔO_2 /Ar water is brought from depth to the surface. Entrainment is thus a concern within the context of this thesis and must be quantified. For simplicity, this discussion begins deriving a mass balance solely focusing on oxygen fluxes and also because more oxygen profiles data is available for analysis. The change in ML oxygen concentration over time may be derived by Eq. (2) where final units are expressed in mol O_2 m^{-2} d^{-1} with h equaling ML depth, F_E representing the entrainment flux, and F_{A-W} as air-water flux.

$$0 = h\frac{dO_2}{dt} = F_E + F_{A-W} + NOP \quad (2)$$

With a residence time of 32 days with respect to gas exchange (h ≈ 193 m, k_{O2} ≈ 6 m d^{-1}) and rapidly changing ML depth in winter, one might expect oxygen within my study area may not reach steady state (Nicholson et al., 2012). Station 3 (29.99ºN 146.40ºE) and station 23 (30.07ºN 146.96ºE) were chosen to check for change in mean ML O_2, because the stations were relatively close spatially and far temporally. Mean ML O_2 at station 23 subtracted by mean ML O_2 at station 3 produced a difference of 1.28 ± 1.10 µmol kg^{-1}. Slight ML stratification observed at Station 23 generated large variation between the means. A two-tailed t-test (α=0.05) confirmed there is not enough evidence to reject the difference in oxygen means between stations equals zero. The steady state assumption is rendered valid.

The mass balance oxygen flux due to entrainment is difference in mean ML oxygen concentration ($[O_2]_{ML}$) and oxygen concentration measured directly below the ML ($[O_2]_D$) as a function of change in ML depth over time (dh/dt) (Eq. 3).

$$F_{E_{O_2}} = -\frac{dh}{dt}\left([O_2]_{ML} - [O_2]_D\right) \quad (3)$$

The negative in front of the right hand side of Equation (4) defines the direction of flux to be within the reference frame of the ML. Negative F_E translates to oxygen leaving the ML to depth. An oxygen residence time (32 d) marked the change in time between final and initial ML deepening. Changes in (dh/dt) were estimated during months of February 2004-2009 from Kuroshio Extension Observatory mooring data published by Cronin et al. (2013) then averaged over the five years resulting in dh/dt= 2.27 m d^{-1}.

F_{A-W} is given by k_{o2} and the air-water oxygen gradient (Eq. 4).

$$F_{A-W_{O_2}} = -k_{O_2}\left([O_2]_{ML} - [O_2]_{sat}\right) \quad (4)$$

The gas transfer velocity for oxygen k_{O2} (m d^{-1}) is a function of oxygen molecular diffusion and kinematic viscosity of seawater at a given salinity and temperature as expressed by the Schmidt number (Sc) and its relation to wind speed (U) (Eq. 5).

$$k_{O2} = (0.222U^2+0.333U)\times(Sc/600)^{-1/2} \quad (5)$$

The first parenthetical term in Eq. 6 was referenced from Nightingale et al. (2000). The oxygen coefficients and equation from table A1 of Wanninkhof (1992) were used to calculate Sc for oxygen.

Like in Eq. 3, the negative in front of the right hand side of Eq. 4 defines oxygen flux within the ML reference frame. A negative flux is leaving the mixed layer to the atmosphere. With this

defined mass balance, NOP can then theoretically be derived taking into account entrainment biases. Entrainment was determined to equal -93 ± 89 and air-sea flux was equal to 70 ± 80 mmol C m^{-2} d^{-1}. D. Lockwood's submitted thesis from continuous data in the KE region during winter reports oxygen supplied to the ML from physical process within the same order of magnitude as the gross oxygen budget reported here (50 mmol O_2 m^{-2} d^{-1}).

Another oxygen budget using O_2/Ar budget was created to check for any significant differences between the methods now that physically introduced oxygen will no longer be considered in the budget. Subtracting oxygen and argon normalized by their respective degrees of saturation derives solely biologically produced oxygen mass balance terms in context of the ML-deep interface (Eq. 6) and air-water interface (Eq. 7)

$$F_{E_{O_2/Ar}} = -\frac{dh}{dt}\left\{\left([O_2]_D - [O_2]_{ML}\right) - \left([Ar]_{ML} - [Ar]_D\right)\frac{[O_2]_{sat}}{[Ar]_{sat}}\right\} \quad (6)$$

$$F_{A\text{-}WO2/Ar} = -k_{O2}(\Delta O_2 - \Delta Ar)[O_2]_{sat} \quad (7)$$

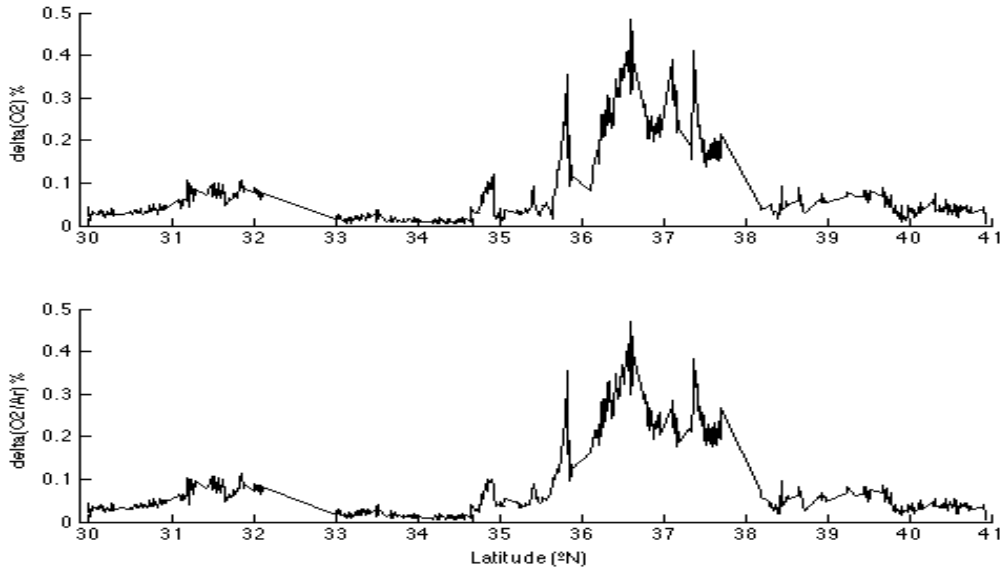

Figure 5. Underway air-sea gas exchange of O_2 calculated using an oxygen mass balance (top) and oxygen/argon mass balance (bottom). Variation is influenced the most by a storm that occurred between 36 and 38 degrees latitude north. The variation is also as great as the calculated mean of the values across the transect.

High wind speed variations create a large variability in the has exchange flux resulting in the mean values of the air water exchange and entrainment fluxes being the same within the errors of the flux terms and render a conclusive NOP estimate impossible with current data. K. Giesbrecht et al. (Biological productivity along Line P in the subarctic north- east Pacific: In-situ versus incubation-based methods, sub- mitted to Global Biogeochemical Cycles, 2012) reported ΔO_2 /Ar-estimated NCP from Station Papa (50°N, 145°W) February, June, and August of 2007–2009. Winter entrainment caused two of the three February NCP estimates to be negative over the three-year study. Net heterotrophy can overpower low ΔO_2/Ar even after the impact of entrainment on ML budget is quantified.

CONCLUSIONS

Winter entrainment events and high wind variability with limited profile data obscure ML oxygen mass budgets. Gas exchange, respiration,

and entrainment contributions to the O2/Ar mass balance are not easily constrained, so calculation of NCP is not attempted. This thesis supports the investment of deploying Argo floats into the KE region. Argo floats deployed in concurrence with this thesis were equipped with highly calibrated oxygen sensors. Long-term oxygen profile data will better constrain the winter ML mass budget in the KE by quantifying change in h over time and air-sea gas exchange changes seasonally.

ACKNOWLEDGEMENTS

Steven Emerson, Hilary Palevsky, and Charles Stump receive my sincerest thanks for helping to complete this thesis and guiding me throughout the process. NSF funding, the captain and crew of the *R/V Melville*, and my fellow classmates deserve acknowledgement in aiding data collection.

REFERENCE LIST

Ayers, J., and M. Lozier. 2010. Physical controls on the seasonal migration of the North Pacific Transition Zone Chlorophyll Front. J. Geophys. Res. **115:** C05001, doi:10.1029/2009JC005596

Benson, B. B., and D. Krause. 1984. The concentration and isotopic fractionation of oxygen dissolved in freshwater and seawater in equilibrium with the atmosphere. Limnol. Oceanogr. **29:** 620-632.

Carpenter, J. 1965. The Chesapeake Bay Institute technique for the Winkler dissolved oxygen method. Limnol. Oceanogr. **10:** 141–143, doi:10.4319/lo.1965.10.1.0141

Cronin, M. F., N. A. Bond, J. T. Farrar, H. Ichikawa, S. R. Jayne, Y. Kawai, M. Konda, B. Qiu, L. Rainville, and H. Tomita. 2013. Formation and erosion of the seasonal thermocline in the Kuroshio Extension Recirculation Gyre. Deep-sea Res. II **85:** 62-74.

Emerson, S., P. Quay, D. Karl, C. Winn, L. Tupas, and M. Landry. 1997. Experimental determination of the organic carbon flux from open ocean surface waters. Nature **389:** 951–954, doi:10.1038/40111

Garcia, H. E., and L. I. Gordon. 1992. Oxygen solubility in seawater: better fitting equations. Limnol. Oceanogr. **37**: 1307–1312.

Hamme, R. C., and S. R. Emerson. 2004. The solubility of neon, nitrogen and argon in distilled water and seawater. Deep-Sea Res. I **51:** 1517-1528, doi:10.1016/j.dsr.2004.06.009

Hamme, R. C., N. Cassar, V. P. Lance, R. D. Vaillancourt, M. L., Bender, P. G. Strutton, T. S. Moore, M. D. DeGrandpre, C. L. Sabine, D. T. Ho, and B. R. Hargreaves. 2012. Dissolved O2/Ar and other methods reveal rapid changes in productivity during a Lagrangian experiment in the Southern Ocean. J. Geophys. Res. **117:** C00F12, doi:10.1029/2011JC007046

Howard, E., S. Emerson, and S. Bushinsky. 2010. Net oxygen production at the subarctic subtropical boundary in the North Pacific, Limnol. Oceanogr. **55:** 2585-2596.

Juranek, L. 2007. Assessment of Pacific Ocean organic carbon production and export using measurements of dissolved oxygen isotopes and oxygen/argon gas ratios. Ph.D. thesis. Univ. of Washington.

Keeling, R.F., S.C. Piper, A.F. Bollenbacher, and J.S. Walker. 2009. Atmospheric CO2 records from sites in the SIO air sampling network. In Trends: A Compendium of Data on Global Change. Carbon Dioxide Information Analysis Center, Oak Ridge National Laboratory, U.S. Department of Energy, Oak Ridge, Tenn., U.S.A., doi: 10.3334/CDIAC/atg.035

Nicholson, D. P., H. R. Stanley, E. Barkan, D. M. Karl, B. Luz, P. D. Quay, and S. C. Doney. 2012. Evaluating triple oxygen isotope estimates of gross primary production at the Hawaii Ocean Time-series and Bermuda Atlantic Time-series Study sites. J. Geophys. Res. **117:** C05012, doi:10.1029/2010JC006856

Nightingale, P., and others. 2000. In situ

evaluation of air–sea gas exchange parameterizations using novel conservative and volatile tracers. Glob. Biogeochem. Cycles **14:** 373–387, doi:10.1029/1999GB900091

Polovina, J., E. Howell, D. Koybayashi, and M. Seki. 2001. The transition zone chlorophyll front, a dynamic global feature defining migration and forage habitat for marine resources. Prog. Oceanogr. **49:** 469–483, doi:10.1016/S0079-6611(01)00036-2

Qiu, B., S. Chen, and P. Hacker. 2007. Effects of mesoscale eddies on subtropical mode water variability from the Kuroshio Extension System Study (KESS), J. Phys. Oceanogr. **37:** 982-1000.

Sabine, C. L., R. A. Feely, N. Cruber, R. M. Key, K. Lee, J. L. Bullister, R. Wanninkhof, C. S. Wong, D. W. R. Wallace, B. Tilbrook, F. J. Millero, T. Peng, A. Kozyr, T. Ono, and A. F. Rios. The Oceanic Sink for Anthropogenic CO2. Science **305:** 367-371, doi:10.1126/science.1097403

Takahashi, T., and others. 2009. Climatological mean and decadal change in surface ocean pCO2, and net sea–air CO2 flux over the global oceans. Deep-Sea Res. II **56:** 554–557, doi:10.1016/j.dsr2.2008.12.009

Volk, T., and M. Hoffert. 1985. Ocean carbon pumps: Analysis of relative strengths and efficiencies in ocean-driven atmospheric changes, 99–110. In E. Sundquist and W. Broecker [eds.], The carbon cycle and atmospheric CO2: Natural variations Archean to present. Geophys. Monogr. Am. Geophys. Union **32**.

Wanninkhof, R. 1992. Relationship between wind speed and gas exchange over the ocean. J. Geophys. Res. **97:** 7373–7382, doi:10.1029/92JC0018